A Misalignment-Tolerant Series-Hybrid Wireless EV Charging System With Integrated Magnetics

Lei Zhao, *Student Member, IEEE*, Duleepa J. Thrimawithana, *Senior Member, IEEE*, Udaya Kumara Madawala, *Fellow, IEEE*, Aiguo Patrick Hu, *Senior Member, IEEE*, and Chunting Chris Mi, *Fellow, IEEE*

***Abstract*—Electric vehicles (EVs) are becoming increasingly popular as a mean of mitigating issues associated with fossil fuel consumption in transportation systems. A wireless inductive power transfer (IPT) interface between EV and the utility grid has several key advantages, such as safety, convenience, and isolation. However, physical misalignments between the pads of IPT charging systems used in EVs are unavoidable and cause variations in key system parameters, significantly increasing losses and affecting power throughput. This paper presents a novel series-hybrid topology in which the series inductors of the primary and pick-up inductor–capacitor–inductor (*LCL*) networks are integrated into polarized magnetic couplers to improve the system performance under pad misalignment. A mathematical model is developed to investigate the behavior of the proposed system under misalignment. To demonstrate the viability of the proposed method, the results of a 3.3-kW prototype series-hybrid IPT system are presented, benchmarked against a conventional IPT system. Experimental results clearly indicate that the proposed system maintains the output power within $\pm 5\%$ of its rated power despite the pad misalignment. The proposed system is efficient, reliable, and cost effective in comparison to conventional *LCL*- and *CL*-compensated IPT systems.**

***Index Terms*—Electric vehicle (EV), inductive power transfer (IPT), misalignment.**

I. Introduction

Electric vehicles (EVs) are regarded as one of the preferred technologies to solve issues associated with increasing fossil fuel usage in transportation systems. Over the last two decades, wireless power transfer technologies have been implemented for EV charging systems using both capacitive and inductive power coupling, of which the latter is commonly referred to as inductive power transfer (IPT) technology [1]–[5]. In its current state, IPT facilitates both uni- and bi-directional power transfer, over small and large air gaps, and at power levels ranging up to tens of kilowatts, and efficiencies as high as 96% [6]–[9]. It is safe, environmentally inert, convenient, and reliable. Applications of IPT technology continues to grow, where static wireless charging and dynamic wireless charging of EVs are two of the most recent developments [10]–[12].

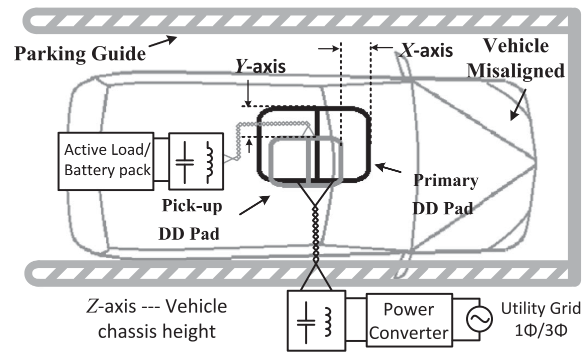

Fig. 1. Typical EV stationary charging system.

A typical wireless EV charging system based on IPT technology is shown in Fig. 1. It illustrates the lateral (X), longitudinal (Y), and vertical (Z) misalignments between the primary and pick-up pads under practical operating conditions. These misalignments cause changes in the self- and mutual-inductances of the coils, which in turn may result in instability, reduction in power transfer, and increase in power losses. Therefore, to mitigate this problem, a variety of mechanisms, such as video and infrared guidance, special mechanical or electronic maneuvering of the primary/pick-up pad and printed guidelines, have been used to date. However, such techniques invariably increase the cost of construction and maintenance. In addition, parking with perfect alignment would have a negative impact on the user acceptance of the wireless charging technology. Therefore, the development of low-cost and reliable circuit topologies and control techniques that enable IPT systems to operate efficiently under misaligned conditions has become a critical component in the design process of practical wireless EV charging systems.

A number of new control concepts have been proposed in [12]–[15] to maintain a stable charging profile under detuned conditions caused by pad misalignment. The controller, usually together with the RF communication, regulates the power flow between the stationary charger and the EV under misalignment. However, regardless of the extra costs, the speed and accuracy of the controllers and the communications could introduce re-

Manuscript received November 17, 2017; revised February 7, 2018; accepted April 3, 2018. Date of publication April 19, 2018; date of current version December 7, 2018. Recommended for publication by Associate Editor O. C. Onar. *(Corresponding author: Lei Zhao.)*

L. Zhao, D. J. Thrimawithana, U. K. Madawala, and A. P. Hu are with the Department of Electrical and Computer Engineering, The University of Auckland, Auckland 1010, New Zealand (e-mail: lzha915@aucklanduni.ac.nz; d.thrimawithana@auckland.ac.nz; u.madawala@auckland.ac.nz; a.hu@auckland.ac.nz).

C. C. Mi is with the Department of Electrical and Computer Engineering, San Diego State University, San Diego, CA 92182 USA (e-mail: cmi@sdsu.edu).

Color versions of one or more of the figures in this paper are available online at http://ieeexplore.ieee.org.

Digital Object Identifier 10.1109/TPEL.2018.2828841

liability issues. The preferred approach to improve tolerance to misalignment relies on the design of improved magnetic pads, such as Double-D (DD), bipolar and tripolar pads proposed in [16]–[18]. These pad designs offer a relatively uniform magnetic field distribution, reducing the changes in self-inductance of the pads and the mutual inductance between the pads during misalignment. As an alternative solution, novel compensation and circuit topologies, which improve the performance of IPT systems operated under misaligned conditions, have recently been introduced [19], [20]. For example in [19], a capacitor–capacitor–inductor compensation network was used to maintain a constant power throughput. However, the prototype was built using a square-shaped secondary pad respective to a larger rectangular primary pad. This asymmetry pad layout reduced the changes in self- and mutual-inductance, thus significantly contributing to the uniform power flow observed. Novel integrated circuit topologies, which also use novel pad designs, are reported in [21]–[23]. In [21]–[23], both the power density and transfer efficiency are improved using DD pads with an integrated compensation inductor. Additionally, the prototype presented in [21]–[23] uses a dual-coupled *LCC* topology implemented using four circular pads to improve the power transfer under misalignment and detuned operation. Some of the most recent developments are reported in [24]–[26], and these solutions consist of a dedicated controller, optimized pad layouts, and optimized compensation networks. However, these solutions utilized sensors and closed-loop controllers for power regulation under misalignment, increasing the system complexity and cost.

Instead of using sensors and closed-loop controllers, a parallel hybrid IPT EV charging system, which is tolerant to 3-D pad misalignments, was proposed in [27]. Both the primary and pick-up employed inductor–capacitor–inductor (*LCL*) and capacitor–inductor (*CL*) compensation networks which were fed by the same converter but connected separately to each of the windings of a bipolar pad. Due to complementary characteristics of *LCL* and *CL* compensation networks, variations in self- and mutual-inductance introduced by pad misalignments have slight impacts on both the real- and reactive-power throughput within its operating region. Therefore, the system in [27], which did not employ a power regulator, exhibited a relatively constant power and efficiency profile over 7% and 100% variation in self- and mutual inductances, respectively. The application of the same topology with Double-D-Quadrature (DDQ) pads in a dynamic charging system was proposed in [28]. However, when the pads move out of the operating region, the current in the primary *CL* compensation network increases exponentially and can easily exceed the ratings of the device. The current increase is caused by the decrease in reflected impedance with increasing distance between the pads. Although this increase in current can be controlled using a closed-loop controller, it significantly deteriorates the system efficiency and may reduce the system reliability, particularly, when used in dynamic charging applications.

This paper presents a novel series-hybrid compensation topology with integrated magnetics to improve misalignment tolerance of IPT systems. The proposed compensation topology eliminates the aforementioned drawbacks associated with [27], by passively limiting the exponential increase in current when the pick-up pad moves out of the operating region. To demonstrate the validity of the proposed concept, a mathematical model is presented first, which characterizes the behavior of the proposed IPT system. The changes in inductances, as well as the main-, cross-, and inter-coupling between the coils of the DD-type primary and pick-up pads, are analyzed to show that a constant charging profile can be maintained over a larger operating region. Finally, the theoretical performance and experimental results of a prototype 3.3-kW system are presented to verify the viability of the proposed topology and its ability to maintain system robustness when the pick-up pad moves out of the operating region.

II. Proposed Series-Hybrid IPT Topology

A. Design and Operating Principles

As can be seen from Fig. 2, a capacitor $C_{pi,2}$ is utilized to partially tune one of the coils $L_{pt,2}$, of the primary DD pad [16]–[18]. This partially tuned *CL* compensation network is connected in series with the fully compensated parallel tuned compensation network formed by the second coil $L_{pt,1}$, of the primary DD pad with $C_{pi,1}$ and $C_{pt,1}$. The residual inductance of the partially tuned $L_{pt,2}$, together with the $L_{pt,1}, C_{pi,1}$, and $C_{pt,1}$, forms an equivalent fully compensated *LCL* network [29]. The pick-up utilizes an identical compensation topology together with a diode rectifier. Alternatively, the pick-up may employ a synchronous rectifier to improve the power transfer efficiency and to enable bidirectional power flow. Accordingly, this new topology allows the integration of the series ac inductor found in a traditional *LCL*-compensated IPT system with the primary/pick-up pad, thus reducing the cost and component count in comparison to the topologies proposed in [27] and [28].

The proposed series-hybrid topology also offers improved tolerance against misalignment. For example, if the magnetic coupling between the pads is reduced due to misalignment, it will cause the reflected impedance across $L_{pt,2}$ to reduce while inducing a larger reflected impedance across the $L_{pt,1}$. This in turns leads to a reduction in power transferred through $L_{pt,2}$, but increases the power through $L_{pt,1}$. The result is a nearly constant charging profile within its designed operating region. Furthermore, in contrast to hybrid tuning topologies proposed in [27] and [28], the *LCL* compensated coil of the new system is connected in series with the *CL*-compensated coil. As such, the *LCL* compensation network passively limits the exponential increase in current in series-connected *CL* compensated coil, when the pick-up pad moves out of the operating region. The intercoupling M_{13} between *LCL*-compensated DD coil $L_{pt,1}$ and *CL*-compensated DD coil $L_{pt,2}$ of the series-hybrid compensation topology further minimize the circulating currents in both coils of the DD pad, as the pick-up pad moves away from the primary.

B. Equivalent Circuit Model

An equivalent circuit of the proposed series-hybrid IPT system is shown in Fig. 3. The DD pads in the primary and pick-up

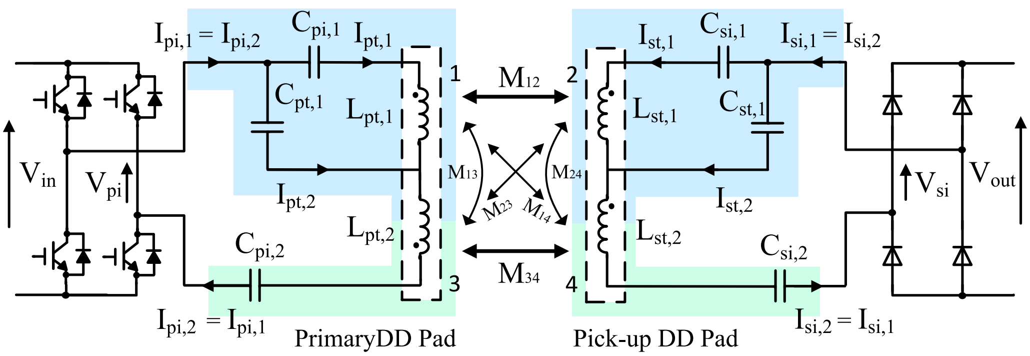

Fig. 2. Proposed novel series-hybrid compensation topology.

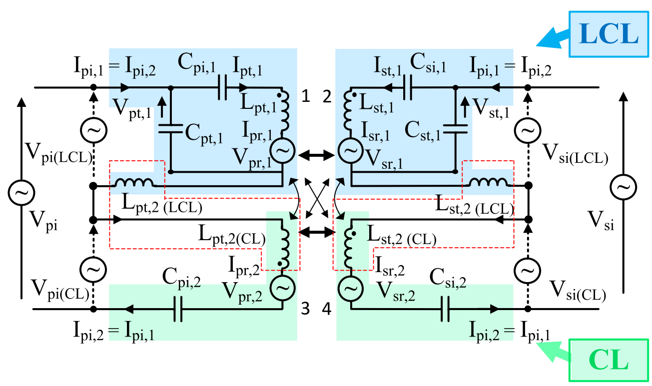

Fig. 3. Equivalent circuit of the proposed series-hybrid compensation topology.

sides are modeled as four separate coils $L_{pt,1}$, $L_{pt,2(CL)}$, $L_{st,1}$, and $L_{st,2(CL)}$ with main couplings M_{12} and M_{34}, intercouplings M_{13} and M_{24}, and cross couplings M_{14} and M_{23}. The residual inductance of $L_{pt,2}$ is modeled as series inductor $L_{pt,2(LCL)}$ together with the $C_{pi,1}$, $C_{pt,1}$, and $L_{pt,1}$ to form a fully tuned *LCL*-compensated network. The reflected voltages $V_{pr,1}$, $V_{pr,2}$, $V_{sr,1}$, and $V_{sr,2}$ relate to the currents in the DD pads due to the coupling between the coils. The pick-up side is identical to the primary and hence modeled similarly.

The inductance of the coil $L_{pt,2}$ is divided into two portions, $L_{pt,2(LCL)}$ and $L_{pt,2(CL)}$. The compensation networks are tuned in such a manner that at the nominal operating point when the pick-up DD pad is placed 120 mm directly above the primary DD pad, the capacitor, $C_{pi,2}$, of the *CL*-compensation network negates the impedance of the inductance, $L_{pt,2(CL)}$. Similarly, $C_{si,2}$ negates the impedance of $L_{st,2(CL)}$, which is the *CL*-tuned portion of $L_{st,2}$, as given by

$$2\pi \cdot f_T = \omega_T = \frac{1}{\sqrt{L_{pt,2(CL)} \cdot C_{pi,2}}} = \frac{1}{\sqrt{L_{st,2(CL)} \cdot C_{si,2}}} \tag{1}$$

where f_T is the switching frequency of the primary full-bridge converter.

The residual inductances of the partially tuned, $L_{pt,2}$ and $L_{st,2}$, form the series inductors, $L_{pt,2(LCL)}$ and $L_{st,2(LCL)}$, of primary and pick-up *LCL* networks, respectively. The inductance of the coils $L_{pt,1}$ and $L_{st,1}$ are partially compensated using

TABLE I
PARAMETERS OF THE PROPOSED HYBRID IPT SYSTEM

Parameter	Value	ESR
$L_{pt,1}$	83.57 µH	125 mΩ
$L_{pt,2}$	82.71 µH	130 mΩ
$L_{pt,2\ (CL)}$	61.00 µH	---
$L_{pt,2\ (LCL)}$	21.71 µH	---
$L_{st,1}$	81.85 µH	122 mΩ
$L_{st,2}$	82.56 µH	126 mΩ
$L_{st,2\ (CL)}$	61.00 µH	---
$L_{st,2\ (LCL)}$	21.56 µH	---
$C_{pt,1}$	0.1705 µF	7.6 mΩ
$C_{st,1}$	0.1655 µF	8.3 mΩ
$C_{pi,1}$	0.0664 µF	11.2 mΩ
$C_{si,1}$	0.0645 µF	10.5 mΩ
$C_{pi,2}$	0.0677 µF	11.9 mΩ
$C_{si,2}$	0.0644 µF	12.3 mΩ
V_{in} & V_{out}	280 V	
f	85.0 kHz	
k (at 0, 0, 120mm)	0.28	
Switches	C3M0065090D	

$C_{pi,1}$ and $C_{si,1}$, respectively, to increase the power transferred through the *LCL*-compensated coils. Therefore, at the nominal operating point

$$2\pi \cdot f_T = \omega_T = \frac{1}{\sqrt{L_{pt,2(LCL)} \cdot C_{pt,1}}} = \frac{1}{\sqrt{L_{st,2(LCL)} \cdot C_{st,1}}} \tag{2}$$

$$= \frac{1}{\sqrt{\left(\omega_T L_{pt,1} - \frac{1}{\omega_T C_{pi,1}}\right) \cdot C_{pt,1}}} = \frac{1}{\sqrt{\left(\omega_T L_{st,1} - \frac{1}{\omega_T C_{si,1}}\right) \cdot C_{st,1}}} \tag{3}$$

where

$$L_{pt,2(LCL)} = L_{pt,2} - L_{pt,2(CL)},$$
$$L_{st,2(LCL)} = L_{st,2} - L_{st,2(CL)}.$$

The parameters of a prototype system, including the inductances of the coils at the nominal operating point (0, 0, 120), are given in Table I. The input and output voltages of the prototype are represented by V_{in} and V_{out}, respectively. V_{in} is composed of $V_{\text{in}(LCL)}$ and $V_{\text{in}(CL)}$, where $V_{\text{in}(CL)}$ is a function of the reflected voltage $V_{pr,2}$. Similarly, $V_{\text{out}(CL)}$ is a function of the reflected voltage $V_{sr,2}$, and together with $V_{\text{out}(LCL)}$ forms V_{out}.

III. Mathematical Model

In order to gain an insight to the operating principles of the proposed series-hybrid IPT system, a detailed mathematical model is developed based on the equivalent circuit model in Fig. 3. It should be noted that in applications requiring bidirectional power flow and/or improved efficiency, a synchronous rectifier can be used to replace the diode rectifier employed by the pick-up converter in Fig. 2. Therefore, to generalize the analysis, V_{si} is defined as a phase-modulated voltage that is generated by a synchronous rectifier. In case a diode rectifier is used in the pick-up, the phase modulation, φ_s, can be substituted with 180° to obtain a specific solution. The primary and pick-up side converters can thus be modeled as voltage sources, V_{pi} and V_{si}, as given by

$$V_{pi} = V_{\text{in}} \cdot \frac{4}{\pi} \sum_{n=1,3,\,5\ldots}^{\infty} \frac{1}{n} \cos(n\omega t) \sin\left(\frac{n\varphi_p}{2}\right) \tag{4}$$

$$V_{si} = V_{\text{out}} \cdot \frac{4}{\pi} \sum_{n=1,3\ldots}^{\infty} \frac{1}{n} \cos(n\omega t - n\theta) \sin\left(\frac{n\varphi_s}{2}\right) \tag{5}$$

where φ_s is the phase modulation of the primary converter and "n" represents the numbers of harmonics. If a diode–rectifier is used, the phase angle of V_{si} with respect to V_{pi}, θ is approximately 90° whereas if a synchronous rectifier is used θ is typically set to 90°. $L_{pt,2(CL)}$ and $L_{st,2(CL)}$ shown in Fig. 3 are fixed inductance values, which are independent of misalignment as the changes in pad inductance caused by misalignment are lumped into $L_{pt,2(LCL)}$ and $L_{st,2(LCL)}$. Furthermore, as shown by the equivalent circuit model, $L_{pt,2(CL)}$ and $L_{st,2(CL)}$ are compensated by $C_{pi,2}$ and $C_{si,2}$, respectively. Therefore,

$$V_{pi(LCL)} = V_{pi} - V_{pr,2} \tag{6}$$

$$V_{si(LCL)} = V_{si} - V_{sr,2}. \tag{7}$$

The voltages $V_{pr,2}$ and $V_{sr,2}$ are the reflected voltages on $L_{pt,2}$ and $L_{st,2}$. The currents flowing through the coils of the *CL* networks can be derived as in [2] and [30], which are given by

$$I_{pi,2} = \frac{-I_{pr,1} \cdot Z_{pr} + V_{pi(LCL)}}{(Z_{pr} + Z_{pi,2})} \tag{8}$$

$$I_{si,2} = \frac{-I_{sr,1} \cdot Z_{sr} + V_{si(LCL)}}{(Z_{sr} + Z_{si,2})}. \tag{9}$$

The currents $I_{pr,1}$ and $I_{sr,1}$ are

$$I_{pr,1} = \frac{(j\omega M_{12} \cdot I_{st,1} + j\omega M_{13} \cdot I_{pi,2} + j\omega M_{14} \cdot I_{si,2})}{Z_{pt,1}} \tag{10}$$

$$I_{sr,1} = \frac{(j\omega M_{12} \cdot I_{pt,1} + j\omega M_{23} \cdot I_{pi,2} + j\omega M_{24} \cdot I_{si,2})}{Z_{st,1}}. \tag{11}$$

Similarly, the currents flowing through the coils of the *LCL* networks are derived as follows:

$$I_{pt,1} = \frac{I_{pi,2} \cdot Z_p - V_{pr,1}}{(Z_p + Z_{pt,1})} \tag{12}$$

$$I_{st,1} = \frac{I_{si,2} \cdot Z_s - V_{sr,1}}{(Z_s + Z_{st,1})} \tag{13}$$

where

$$Z_{pc,1} = \frac{1}{j\omega C_{pt,1}} + R_{Cpt,1}, \quad Z_{sc,1} = \frac{1}{j\omega C_{st,1}} + R_{Cst,1}$$

$$Z_{pt,1} = j\omega L_{pt,1} + \frac{1}{j\omega C_{pi,1}} + R_{Lpt,1} + R_{Cpi,1}$$

$$Z_{st,1} = j\omega L_{st,1} + \frac{1}{j\omega C_{si,1}} + R_{Lst,1} + R_{Csi,1}$$

$$Z_{pi,2} = j\omega L_{pt,2} + \frac{1}{j\omega C_{pi,2}} + R_{Lpt,2} + R_{Cpi,2}$$

$$Z_{si,2} = j\omega L_{st,2} + \frac{1}{j\omega C_{si,2}} + R_{Lst,2} + R_{Csi,2}$$

$$Z_p = \frac{Z_{pi,2} \cdot Z_{pc,1}}{Z_{pi,2} + Z_{pc,1}}, \quad Z_s = \frac{Z_{si,2} \cdot Z_{sc,1}}{Z_{si,2} + Z_{sc,1}}$$

$$Z_{pr} = \frac{Z_{pt,1} \cdot Z_{pc,1}}{Z_{pt,1} + Z_{pc,1}}, \quad Z_{sr} = \frac{Z_{st,1} \cdot Z_{sc,1}}{Z_{st,1} + Z_{sc,1}}.$$

$R_{Cpt,1}$, $R_{Cst,1}$, $R_{Lpt,1}$, $R_{Lst,1}$, $R_{Cpi,1}$, $R_{Csi,1}$, $R_{Lpt,2}$, $R_{Lst,2}$, $R_{Cpi,2}$, and $R_{Csi,2}$ represent the resistances of the coils, and inductors and capacitors employed in the two hybrid compensation networks.

The currents flowing through the coils as a function of supply voltages can be derived from (8) to (13) as presented in [2] and [30]. For example, $I_{pi,2}$ can be derived using (8)–(13) as given by

$$\begin{aligned} I_{pi,2} = \frac{1}{K_1} \Bigg[& -j\omega M_{12} \frac{V_{si} Z_s - V_{sr,2} Z_s - V_{sr,1} Z_{si,2}}{(Z_s + Z_{st,1}) Z_{si,2}} Z_{pr} \\ & - \frac{\omega^2 M_{14} M_{12} (V_{pi} Z_p - V_{pr,2} Z_p - V_{pr,1} Z_{pi,2}) Z_{sr} Z_{pr}}{((Z_{sr} + Z_{si,2}) Z_{st,1} + j\omega M_{24} Z_{sr}) (Z_p + Z_{pt,1}) Z_{pi,2}} \\ & + \frac{j\omega M_{14} (V_{si} - V_{sr,2}) Z_{st,1} Z_{pr}}{((Z_{sr} + Z_{si,2}) Z_{st,1} + j\omega M_{24} Z_{sr})} \\ & + (V_{pi} - V_{pr,2}) Z_{pt,1} \Bigg] \end{aligned} \tag{14}$$

where K_1 is given as

$$\begin{aligned} K_1 = & (Z_{pr} + Z_{pi,2}) Z_{pt,1} + j\omega M_{13} Z_{pr} \\ & + \frac{\omega M_{14} \omega M_{23} Z_{sr} Z_{pr}}{((Z_{sr} + Z_{si,2}) Z_{st,1} + j\omega M_{24} \cdot Z_{sr})}. \end{aligned}$$

Similarly, $I_{si,2}$, $I_{pt,1}$ and $I_{st,1}$ can be derived from (8) to (13), but are not shown in this paper due to limited space.

The reflected voltage $\mathbf{V_r}$ consists of $V_{pr,1}, V_{sr,1}, V_{pr,2}$, and $V_{sr,2}$, which can be expressed as

$$\mathbf{V_r} = j\omega \cdot \mathbf{M} \times \mathbf{I} \tag{15}$$

where $\mathbf{M}$ represents the mutual coupling between the coils of the pads, and $\mathbf{I}$ consist of the currents $I_{pi,2}, I_{si,2}, I_{pt,1}$, and $I_{st,1}$.

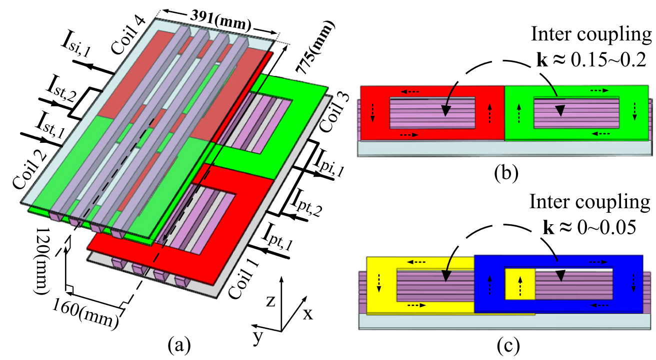

Fig. 4. (a) Pad displacement at (160, 0, 120). (b) Intercoupling for DD pad. (c) Intercoupling for bipolar pad.

The voltages (4)–(7) and the currents can be then substituted into (15) to obtain the reflected voltages $\mathbf{V_r}$. As this mathematical derivation is complicated and tedious, the detailed solution for the reflected voltages $\mathbf{V_r}$ is not presented for clarity, but they are similar to solutions presented in [2] and [30]. The output power can now be derived as given by

$$P_{\text{out}} = -Re : \{V_{si} \cdot I_{si,2}{}^{*}\} . \tag{16}$$

The analysis presented above can be significantly simplified by ignoring the cross coupling between the coils and neglecting the changes in self-inductance of the coils due to misalignment as described in the proceeding section.

IV. System Characteristic Analysis

A. Parameters of the Pads

As the series-hybrid networks are designed to function as ideally tuned *LCL* networks at the nominal operating point, $I_{pi,1}$ is in phase with V_{pi}, while $I_{pt,1}$ lags V_{pi} by 90° [1], [2]. $I_{pt,1}$ and $I_{pi,1}$ are therefore 90° out of phase, and to deliver power to the pick-up through both $L_{pt,1}$ and $L_{pt,2}$ the primary coils are physically connected in opposite polarity, making the coupling M_{34} between coils 3 and 4 negative. Figs. 2 and 4(a) depict the reversed dots next to $L_{pt,1}$ and $L_{pt,2}$ indicating the negative coupling. This also leads to a negative coupling M_{13}, from coils 1 to 3, which in turn increases the input impedance seen by the primary converter when the pick-up pad is not in the vicinity of the primary pad. As a result, when the pick-up pad is not in the vicinity of the primary pad, the current flowing through the *CL*-compensated coil is minimized as given by

$$I_{pi,2} = \frac{V_{pi} \cdot (Z_p + Z_{pt,1})}{\left[Z_{pi,2}\left(Z_p + Z_{pt,1}\right) - j\omega M_{13} \cdot Z_p - \omega^2 M_{13}{}^2\right]}. \tag{17}$$

Bipolar pads, shown in Fig. 4(c), can be used in the proposed series-hybrid IPT system to replace the DD pads. Since the two coils in a bipolar pad are magnetically decoupled, a simplified mathematical model can be derived to describe the behavior of a series-hybrid system with bipolar pads by setting M_{13} and M_{24} to zero in the preceding analysis. However, moving the pick-up pad away from the primary pad will lead to a higher a circulating current in both coils of the bipolar primary pad. A detailed comparison between these two options is presented in Section V.

To illustrate the ability of the proposed hybrid-IPT system to maintain a nearly constant power transfer under misaligned operating conditions, 160-mm-horizontal (*Y*-axis) and 40-mm-vertical (*Z*-axis) displacements of the pick-up pad with reference to the stationary primary pad were considered. The tuned position of the system has been chosen as the location when the pick-up pad is orientated 120 mm directly above the primary pad (0, 0, 120), simulating the average height of a motor vehicle with the orientation for maximum coupling. Therefore, the system exhibits the strongest coupling between the pads when the pick-up pad is located at (0, 0, 100), where k_{12} and k_{34} are approximately 0.35. A significant change in the main coupling is observed with increasing vertical and horizontal displacements, as both k_{12} and k_{34} drop to 0.14 at (160, 0, 140). In contrast, the changes in inter- and cross-coupling are relatively small and constant, which vary from 0.2 to 0.15 and from 0.15 to 0.08, respectively, as the pads are misaligned. It should also be noted that the self-inductance of the coils changes by about 7% across this operating region.

B. Design of a Compensation Network

The relationship between system parameters and power transfer derived in (16) is complex and as a result, only provides a limited insight of the system operation. As such, (16) is simplified by assuming the coupling terms, k_{13}, k_{24} and k_{14}, k_{23}, are zero and both the primary and pick-up compensation networks are tuned to the nominal operating frequency, to obtain

$$P_h = \frac{8 \cdot V_{\text{in}} \cdot V_{\text{out}}}{\pi^2 \cdot \omega \cdot \left(\frac{L_{pt,2(LCL)} \cdot L_{st,2(LCL)}}{k_{12} \cdot \sqrt{L_{pt,1} \cdot L_{st,1}}} + k_{34} \cdot \sqrt{L_{pt,2} \cdot L_{st,2}} \right)}. \tag{18}$$

As evident from (18), the power throughput of the system is proportional to k_{12} and inversely proportional to k_{34}. However, the contribution of k_{12} and k_{34} to power transfer depends on the relative sizes of coil inductances L_{pt1}, L_{st1}, $L_{pt2}, L_{st2}, L_{pt2(LCL)}$, and $L_{pt2(LCL)}$. Therefore, to capture the effect of relative sizes of these inductances as given by (18), a ratio κ_T is defined

$$\kappa_T = \sqrt{\frac{L_{pt,2(LCL)}}{\sqrt{L_{pt,1} \cdot L_{pt,2}}} \cdot \frac{L_{st,2(LCL)}}{\sqrt{L_{st,1} \cdot L_{st,2}}}} \tag{19}$$

where

$$L_{pt,2(LCL)} = L_{pt,2} - \frac{1}{\omega^2 C_{pi,2}},$$

$$L_{st,2(LCL)} = L_{st,2} - \frac{1}{\omega^2 C_{si,2}}.$$

Equation (18) can now be expressed as a function of k_{12}, k_{34}, and κ_T as given by

$$P_h = \frac{8 \cdot V_{\text{in}} \cdot V_{\text{out}} \cdot k_{12}}{\pi^2 \cdot \omega \cdot \sqrt{L_{pt,1} \cdot L_{st,1}} \cdot (\kappa_T{}^2 + k_{12} \cdot k_{34})}. \tag{20}$$

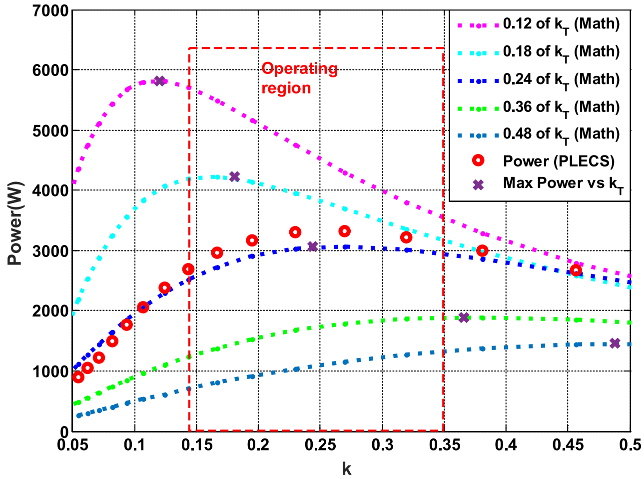

Fig. 5. Power variations against system coupling coefficient.

Using (20), the optimum value of κ_T can be found for a given set of operating parameters. This optimum value of κ_T can be realized by selecting the capacitors $C_{pi,2}$ and $C_{si,2}$ as given in (19). Alternatively, the DD pads can employ coils with different inductances on each coil to achieve a misalignment performance while improving power transfer efficiency.

As a design example, Fig. 5 depicts the power throughput of the system with the parameters listed in Table I, as a function of k_{12}, k_{34}, and κ_T. In this example, since only *Y*-axis and *Z*-axis displacements are considered, k_{12} and k_{34} are approximately of equal value but varies between 0.15 to 0.35. When κ_T changes from 0.12 to 0.24, the variation in power throughput due to k_{12} and k_{34} reduces. However, a further increase in κ_T toward 0.48 results in a decline of system performance as the variation in power throughput with k_{12} and k_{34} increases. Therefore, the optimum value of κ_T is taken as 0.24 for the example system considered in this paper as this results in the lowest variation in power throughput over the operating region indicated in Fig. 5. Once a suitable κ_T is established, the relationship between $L_{pt,2(LCL)}$ and $L_{pt,2}$ can be derived from (19). Since both the primary and pick-up are identical in this specific example, $L_{pt,2(LCL)}$ should be equal to $\kappa_T \cdot L_{pt,2}$. This information can now be used in (1)–(3) to derive the parameters of the components used in the hybrid compensation networks.

The accuracy of the approximation given by (20) is validated by simulating the system in MATLAB PLECS, accounting for coupling terms k_{13}, k_{24} and k_{14}, k_{23} as well as changes in self-inductance of the coils. As evident from Fig. 5, the simulated power throughput of the system with a κ_T of 0.24 closely matches the results obtained from (20), thus validating the accuracy of the analysis presented above. It is also evident that when k_{12} and k_{34} are identical to κ_T, the power throughput is at its maximum as indicated by the crosses in Fig. 5.

C. Series-Hybrid Versus Parallel-Hybrid Compensation Topologies

The operating principles and misalignment tolerances of the topology in [27] and the series-hybrid topology presented in this paper are somewhat similar. Therefore, a side-by-side comparison of the two systems based on a simplified mathematical model is presented to highlight the benefits of the series-hybrid topology. Assuming the coil inductances $L_{pt1}, L_{st1}, L_{pt2}$, and L_{st2} are identical, (18) can be further simplified as

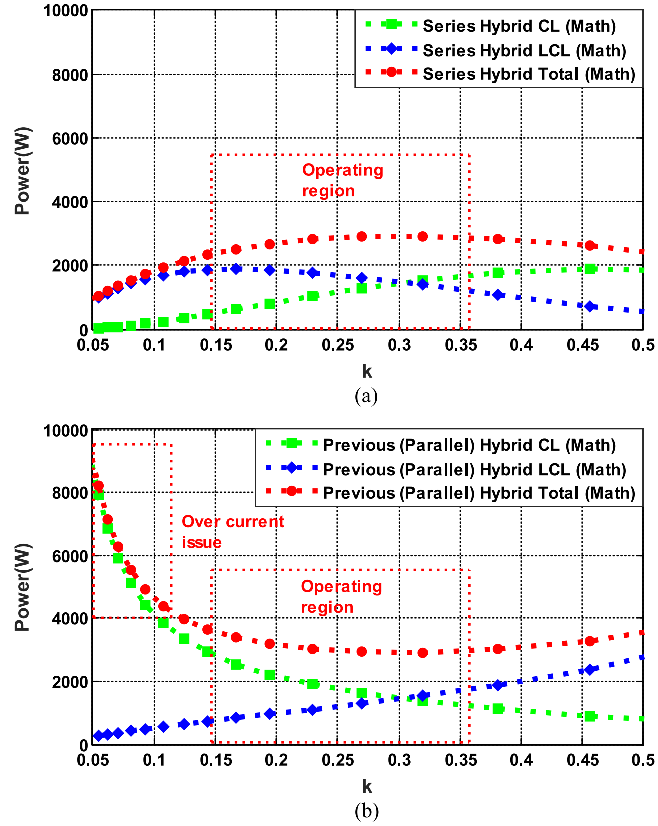

Fig. 6. Power variations against system coupling coefficient. (a) Series hybrid. (b) Previous (parallel) hybrid topology.

$$P_{\text{series}-h} = \frac{8 \cdot V_{\text{in}} V_{\text{out}}}{\pi^2} \cdot \frac{1}{Z_{CL} + Z_{LCL}} \tag{21}$$

where $P_{\text{series}-h}$ is the total combined power transferred through the series-connected *LCL*-compensated, $P_{\text{series}-LCL}$, and the *CL*-compensated, $P_{\text{series}-CL}$, coils of the proposed hybrid system, which are given by

$$P_{\text{series}-LCL} = \frac{8 \cdot V_{\text{in}} V_{\text{out}}}{\pi^2} \cdot \frac{Z_{LCL}}{\left(Z_{CL} + Z_{LCL}\right)^2} \tag{22}$$

$$P_{\text{series}-CL} = \frac{8 \cdot V_{\text{in}} V_{\text{out}}}{\pi^2} \cdot \frac{Z_{CL}}{\left(Z_{CL} + Z_{LCL}\right)^2}. \tag{23}$$

Z_{LCL} and Z_{CL} are defined as follows:

$$Z_{LCL} = \frac{\omega \cdot L_{pt,2}\,(LCL) \cdot L_{st,2}\,(LCL)}{M_{12}}, \quad Z_{CL} = \omega \cdot M_{34}.$$

The power transfer profiles through each coil as well as the combined power throughput of the series-hybrid system are depicted in Fig. 6(a). In contrast, the *CL* and the *LCL* compensation networks of the hybrid system in [27] are connected in parallel across the output of the inverter. The power transfer profiles through each coil as well as the combined power throughput of

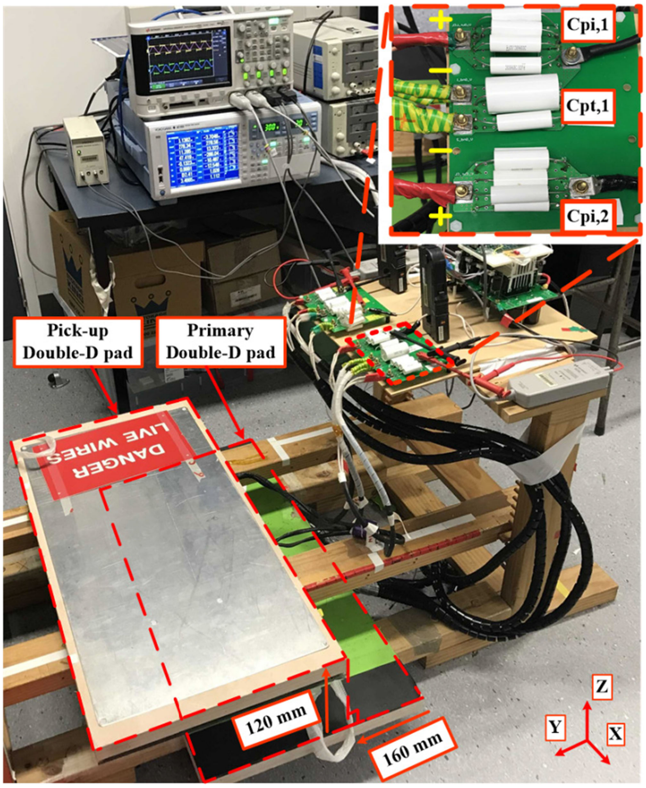

Fig. 7. Experimental setup of the 3.3-kW prototype.

this hybrid system are derived using the mathematical model presented in [27] and are depicted in Fig. 6(b) for comparison.

As evident from Fig. 6(a) and (b), both systems can maintain a nearly constant power output within the operating region. However, the current in the *CL*-tuned coil of the hybrid system in [27] increases exponentially as the pads move away from each other, leading to an exponential increase in power throughput. The higher currents will lead to poor efficiency and eventual system failure of the design in [28] if not controlled using a closed-loop controller. In contrast, the current through both the *LCL*- and *CL*-compensated coils of the new series-hybrid system decreases, causing the power throughput to reduce, as the pick-up pad moves out of the operating region.

V. Experimental Results

In order to verify the viability of the proposed concept, a 3.3-kW series-hybrid IPT system was designed and built, as shown in Fig. 7. The parameters and operating conditions of the prototype system are given in Table I. The primary converter was intentionally operated at a fixed 100% modulation using open-loop controllers to demonstrate the ability of the proposed hybrid IPT system to tolerate pad misalignment.

Figs. 8 and 9 present voltages and currents at (0, 0, 120) and (160, 0, 120), respectively, that were obtained from the theoretical model presented in Section III as well as experimentally. Both mathematical and experimental results are well aligned, which verifies the accuracy of the mathematical model. The input and output currents, $I_{pi,2}$ and $I_{si,2}$, are very similar in

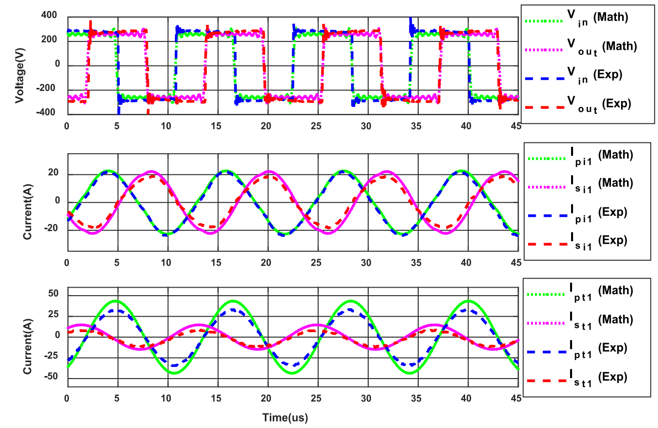

Fig. 8. Current waveforms at the tuned position (0, 0, 120).

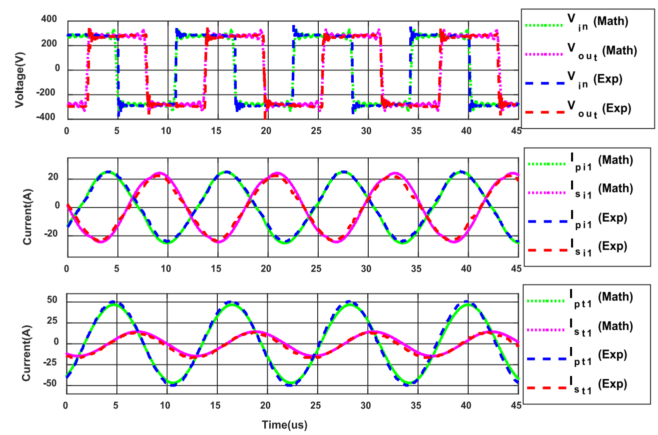

Fig. 9. Current waveforms at the misaligned position (160, 0, 120).

magnitude and shape at both nominal (0, 0, 120) and misaligned (160, 0, 120) positions, indicating that the power throughput of the system is approximately constant. The relatively constant power throughput can be attributed to changes in the reflected voltage $V_{pr,2}$ and $V_{sr,2}$ caused by misalignment. As the pick-up pad moves from (0, 0, 120) to (160, 0, 120), the coupling between windings $L_{pt,2}$ and $L_{st,2}$ decreases, but the current in these coils $I_{pi,2}$ and $I_{si,2}$ remain constant. As a result, when the pads are misaligned, $V_{pr,2}$ and $V_{sr,2}$ decrease causing $I_{pt,1}$ and $I_{st,1}$ to increase as evident from Fig. 9. This increase in the currents increases the power transfer between windings $L_{pt,1}$ and $L_{st,1}$, in order to compensate for the reduction in power transfer between windings $L_{pt,2}$ and $L_{st,2}$. From Figs. 8 and 9, it is also evident that the converter currents are slightly lagging the respective converter voltages to facilitate zero-voltage switching.

Fig. 10 shows the measured and theoretical power output of the series-hybrid IPT system as a function of misalignment to further demonstrate the functionality of the proposed hybrid concept. A conventional *LCL*-compensated IPT system and a *CL*-compensated IPT system, with similar specification and fixed duty-cycle open-loop controllers, have been used as baseline systems to benchmark the performance of the series-hybrid IPT system. The power output of both baseline systems either

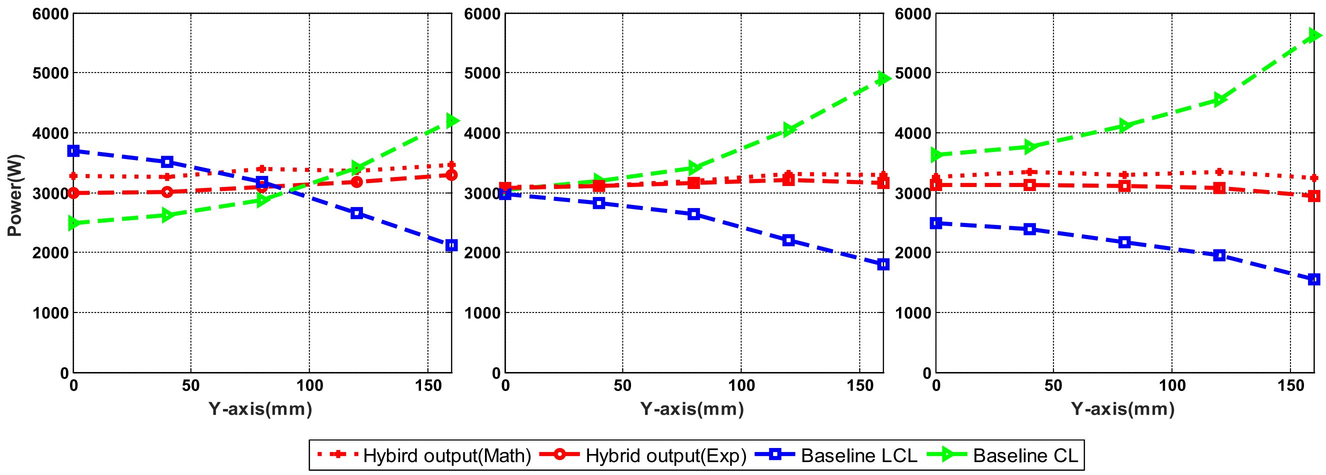

(a) (b) (c)

Fig. 10. Variation in output power of series-hybrid topology due to pad misalignments. (a) *Z*-axis: 100 mm. (b) *Z*-axis: 120 mm. (c) *Z*-axis: 140 mm.

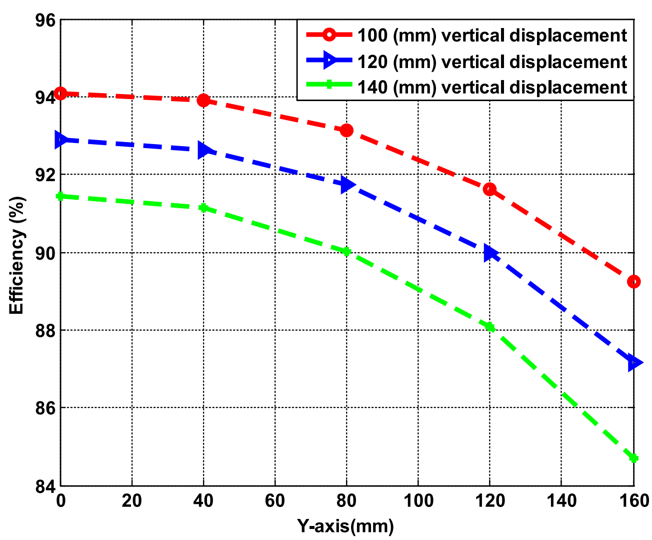

Fig. 11. Variation in efficiency due to pad misalignment.

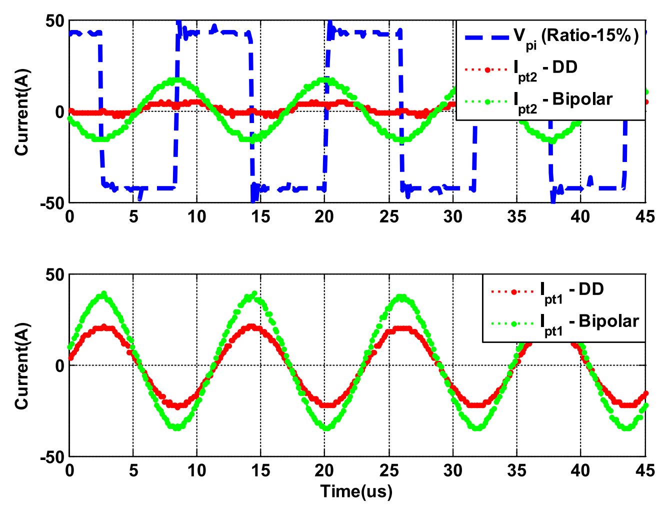

Fig. 12. Primary current waveforms without secondary circuitry.

increases or decreases as a function of the coupling coefficient, with increasing vertical and horizontal displacements. As evident from Fig. 10, the output power of baseline systems changes by up to 100% due to misalignment whereas the proposed system maintains the output power approximately constant under the same conditions. The constant charging characteristics will reduce system complexity and cost in terms of sensors and controllers while improve the reliability of a wireless charging system. It should be noted that a similar power transfer profile is observed when the pick-up pad is moved along the *X*-axis. However, due to changes in cross coupling between adjacent coils of the DD pad employed, the prototype could only maintain a near uniform power transfer from –80 to +120 mm misalignment in the *X*-axis.

Fig. 11 shows the dc–dc (i.e., $V_{\rm in}$ to $V_{\rm out}$) efficiency of the prototype, measured using a Yokogawa WT1800 power analyzer while operating under the conditions shown in Fig. 10. The efficiency varies with both vertical and horizontal displacements and drops as the pick-up pad misaligns with respect to the stationary primary pad. As can be seen from Figs. 8 and 9, the input and output currents remain approximately constant for all displacements considered. But, $I_{pt,1}$ and $I_{st,1}$ increase with increasing misalignment. Hence, the contribution of conduction losses in $L_{pt,1}$ and $L_{st,1}$ significantly increase as the pads misalign, causing a reduction in efficiency. Although the maximum system efficiency achieved by this proof-of-concept prototype is only 94%, it can potentially be improved through the proper design of DD pads and optimizing the system.

As discussed in Section IV, one of the disadvantages of the hybrid IPT system presented in [27] and [28] is the inability to operate the primary converter, when the pick-up is not in the vicinity of the primary pad. However, the proposed series-hybrid IPT system solves this issue by configuring $L_{pt,1}$, and $L_{pt,2}$ to be out of phase as mathematically shown in (17). In order to verify this, the primary of the series-hybrid IPT system is operated alone without the secondary, and the experimental results are shown in Fig. 12. Note that the primary is operated at maximum modulation, mimicking worst case operating conditions. Fig. 12 also compares the behavior of the system when operated with DD pads and bipolar pads to illustrate the significance of a negative M_{13}. As evident from Fig 12, the circulating currents $I_{pi,2}$ and $I_{pt,1}$ are limited to 2.4 and 15.0 $\mathrm{A_{rms}}$, respectively, when using DD pads. However, if bipolar pads are used under the same conditions, $I_{pi,2}$ and $I_{pt,1}$ will increase to 11.6 and 24.9 $\mathrm{A_{rms}}$, respectively. The two coils in a bipolar pad are decoupled, resulting in a zero M_{13}. Therefore, according to (17), a significant circulating current is observed when the pick-up is not present.

VI. Conclusion

This paper proposed a novel series-hybrid compensation topology for IPT-based wireless EV charging systems to achieve improved tolerance to pad misalignment. The proposed system uses the two coils of polarized primary and pick-up pads as series and parallel inductors of the primary and pick-up *LCL* compensation networks, respectively. Each coil was compensated using series compensation capacitors to balance the power transferred through the coils, thus negating the adverse effects introduced by the pad misalignment. A mathematical model has been presented to provide an insight into the performance of the system. Both theoretical and experimental results of a 3.3-kW prototype IPT system convincingly demonstrated that the proposed series-hybrid IPT concept is able to deliver a nearly constant power output within a specified operating region. The prototype system, which was operated at a fixed 100% modulation, maintained the output power within ±5% when the pick-up pad was misaligned from –160 to 160 mm along *Y*-axis, –80 to 120 mm along *X*-axis and –20 to 20 mm along *Z*-axis. These results convincingly demonstrated that the proposed hybrid system offers a cost-effective and reliable solution to pad misalignments in wireless EV charging applications.

References

[1] U. K. Madawala and D. J. Thrimawithana, "A bidirectional inductive power interface for electric vehicles in V2G systems," *IEEE Trans. Ind. Electron.*, vol. 58, no. 10, pp. 4789–4796, Oct. 2011.

[2] D. J. Thrimawithana and U. K. Madawala, "A generalized steady-state model for bidirectional IPT systems," *IEEE Trans. Power Electron.*, vol. 28, no. 10, pp. 4681–4689, Oct. 2013.

[3] M. P. Kazmierkowski and A. J. Moradewicz, "Unplugged but connected: Review of contactless energy transfer systems," *IEEE Ind. Electron. Mag.*, vol. 6, no. 4, pp. 47–55, Dec. 2012.

[4] A. Mohamed, A. Berzoy, and O. Mohammed, "Experimental validation of comprehensive steady-state analytical model of bidirectional WPT system in EVs applications," *IEEE Trans. Veh. Technol.*, vol. 66, no. 7, pp. 5584–5594, Jul. 2017.

[5] N. X. Bac, D. M. Vilathgamuwa, and U. K. Madawala, "A SiC-based matrix converter topology for inductive power transfer system," *IEEE Trans. Power Electron.*, vol. 29, no. 8, pp. 4029–4038, Aug. 2014.

[6] R. Bosshard and J. W. Kolar, "Multi-objective optimization of 50 kW/85 kHz IPT system for public transport," *IEEE J. Emerg. Sel. Topics Power Electron.*, vol. 4, no. 4, pp. 1370–1382, Dec. 2016.

[7] S. R. Hui, "Magnetic resonance for wireless power transfer [A look back]," *IEEE Power Electron. Mag.*, vol. 3, no. 1, pp. 14–31, Mar. 2016.

[8] J. M. Miller *et al.*, "Demonstrating dynamic wireless charging of an electric vehicle: The benefit of electrochemical capacitor smoothing," *IEEE Power Electron. Mag.*, vol. 1, no. 1, pp. 12–24, Mar. 2014.

[9] S. Bandyopadhyay, V. Prasanth, P. Bauer, and J. Ferreira, "Multi-objective optimisation of a 1-kW wireless IPT systems for charging of electric vehicles," in *Proc. IEEE Transp. Electrif. Conf. Expo*, 2016, pp. 1–7.

[10] S. Y. Choi, B. W. Gu, S. Y. Jeong, and C. T. Rim, "Advances in wireless power transfer systems for roadway-powered electric vehicles," *IEEE J. Emerg. Sel. Topics Power Electron.*, vol. 3, no. 1, pp. 18–36, Mar. 2015.

[11] C. C. Mi, G. Buja, S. Y. Choi, and C. T. Rim, "Modern advances in wireless power transfer systems for roadway powered electric vehicles," *IEEE Trans. Ind. Electron.*, vol. 63, no. 10, pp. 6533–6545, Oct. 2016.

[12] S. Ruddell, U. K. Madawala, D. J. Thrimawithana, and M. Neuburger, "A novel wireless converter topology for dynamic EV charging," in *Proc. IEEE Transp. Electrif. Conf. Expo*, 2016, pp. 1–5.

[13] M. J. Neath, A. K. Swain, U. K. Madawala, and D. J. Thrimawithana, "An optimal PID controller for a bidirectional inductive power transfer system using multiobjective genetic algorithm," *IEEE Trans. Power Electron.*, vol. 29, no. 3, pp. 1523–1531, Mar. 2014.

[14] J. M. Miller, O. C. Onar, and M. Chinthavali, "Primary-side power flow control of wireless power transfer for electric vehicle charging," *IEEE J. Emerg. Sel. Topics Power Electron.*, vol. 3, no. 1, pp. 147–162, Mar. 2015.

[15] F. F. Van Der Pijl, M. Castilla, and P. Bauer, "Adaptive sliding-mode control for a multiple-user inductive power transfer system without need for communication," *IEEE Trans. Ind. Electron.*, vol. 60, no. 1, pp. 271–279, Jan. 2013.

[16] M. Budhia, J. T. Boys, G. A. Covic, and C.-Y. Huang, "Development of a single-sided flux magnetic coupler for electric vehicle IPT charging systems," *IEEE Trans. Ind. Electron.*, vol. 60, no. 1, pp. 318–328, Jan. 2013.

[17] A. Zaheer, H. Hao, G. A. Covic, and D. Kacprzak, "Investigation of multiple decoupled coil primary pad topologies in lumped IPT systems for interoperable electric vehicle charging," *IEEE Trans. Power Electron.*, vol. 30, no. 4, pp. 1937–1955, Apr. 2015.

[18] S. Kim, G. A. Covic, and J. T. Boys, "Tripolar pad for inductive power transfer systems for EV charging," *IEEE Trans. Power Electron.*, vol. 32, no. 7, pp. 5045–5057, Jul. 2017.

[19] J. L. Villa, J. Sallan, J. F. S. Osorio, and A. Llombart, "High-misalignment tolerant compensation topology for ICPT systems," *IEEE Trans. Ind. Electron.*, vol. 59, no. 2, pp. 945–951, Feb. 2012.

[20] J. Hou, Q. Chen, X. Ren, X. Ruan, S.-C. Wong, and K. T. Chi, "Precise characteristics analysis of series/series-parallel compensated contactless resonant converter," *IEEE J. Emerg. Sel. Topics Power Electron.*, vol. 3, no. 1, pp. 101–110, Mar. 2015.

[21] W. Li, H. Zhao, S. Li, J. Deng, T. Kan, and C. C. Mi, "Integrated LCC compensation topology for wireless charger in electric and plug-in electric vehicles," *IEEE Trans. Ind. Electron.*, vol. 62, no. 7, pp. 4215–4225, Jul. 2015.

[22] T. Kan, T.-D. Nguyen, J. C. White, R. K. Malhan, and C. C. Mi, "A new integration method for an electric vehicle wireless charging system using LCC compensation topology: Analysis and design," *IEEE Trans. Power Electron.*, vol. 32, no. 2, pp. 1638–1650, Feb. 2017.

[23] F. Lu, H. Zhang, H. Hofmann, and C. Mi, "A dual-coupled LCC-compensated IPT system to improve misalignment performance," in *Proc. IEEE PELS Workshop Emerg. Technol. Wireless Power Transf.*, 2017, pp. 1–8.

[24] A. Kamineni, M. J. Neath, G. A. Covic, and J. T. Boys, "A mistuning-tolerant and controllable power supply for roadway wireless power systems," *IEEE Trans. Power Electron.*, vol. 32, no. 9, pp. 6689–6699, Sep. 2017.

[25] J. Shin *et al.*, "Design and implementation of shaped magnetic-resonance-based wireless power transfer system for roadway-powered moving electric vehicles," *IEEE Trans. Ind. Electron.*, vol. 61, no. 3, pp. 1179–1192, Mar. 2014.

[26] S. Zhou and C. C. Mi, "Multi-paralleled LCC reactive power compensation networks and their tuning method for electric vehicle dynamic wireless charging," *IEEE Trans. Ind. Electron.*, vol. 63, no. 10, pp. 6546–6556, Oct. 2016.

[27] L. Zhao, D. Thrimawithana, and U. Madawala, "A hybrid bi-directional wireless EV charging system tolerant to pad misalignment," *IEEE Trans. Ind. Electron.*, vol. 64, no. 9, pp. 7079–7086, Sep. 2017.

[28] L. Zhao, S. Ruddell, D. J. Thrimawithana, U. K. Madawala, and P. A. Hu, "A hybrid wireless charging system with DDQ pads for dynamic charging of EVs," in *Proc. IEEE PELS Workshop Emerg. Technol. Wireless Power Transf.*, 2017, pp. 1–6.

[29] B. Esteban, N. Stojakovic, M. Sid-Ahmed, and N. C. Kar, "Development of mutual inductance formula for misaligned planar circular spiral coils," in *Proc. IEEE Energy Convers. Congr. Expo.*, 2015, pp. 1306–1313.

[30] Y. Song, U. K. Madawala, D. J. Thrimawithana, and A. P. Hu, "LCL and CL compensations for wireless three phase bi-directional EV charging systems," in *Proc. IEEE Annu. Southern Power Electron. Conf.*, 2016, pp. 1–6.

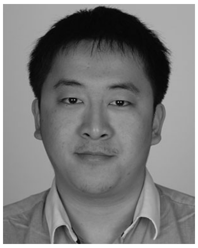

Lei Zhao (S'14) received the B.Sc. Eng. degree in electrical engineering from the Xi'an University of Technology, Xi'an, China, in 2011, and the M.Sc. Eng. degree in electrical engineering from The University of Auckland, Auckland, New Zealand, in 2013, where he is currently working toward the Ph.D. degree in power electronics from 2014.

His research interests mainly focused on the optimization of the bidirectional inductive power transfer, which could be implemented to the incoming electric vehicles and vehicle-to-grid systems.

Duleepa J. Thrimawithana (M'09–SM'18) received the B.E. degree in electrical engineering (with first class hons.) and the Ph.D. degree in power electronics from The University of Auckland, Auckland, New Zealand, in 2005 and 2009, respectively.

He joined the Department of Electrical and Computer Engineering, The University of Auckland, in 2009, where he is currently a Senior Lecturer. He has coauthored more than 100 international journal and conference publications, and has filled 14 patents on wireless power transfer technologies. His main research interests include wireless power transfer, power electronics, and renewable energy.

Dr. Thrimawithana serves as the Chairman of the Joint Chapter of IEEE Industrial Electronics and Industrial Applications Society, New Zealand (North). In recognition of his outstanding contributions to engineering as an Early Career Researcher, he received the Jim and Hazel D. Lord Fellowship in 2014.

Udaya Kumara Madawala (S'88–M'93–SM'06–F'18) received the B.Sc. (hons.) degree in electrical engineering from the University of Moratuwa, Moratuwa, Sri Lanka, in 1986, and the Ph.D. degree in power electronics from The University of Auckland, Auckland, New Zealand, in 1993, as a Commonwealth Doctoral Scholar.

He is currently a Full Professor. He has more than 250 IEEE and IET journal and international conference publications, and holds a number of patents related to wireless power transfer and power converters. His research interests include power electronics, wireless power transfer, vehicle-to-grid applications, and renewable energy.

Dr. Madawala is a Distinguished Lecturer of the IEEE Power Electronic Society, and has more than 30 years of both industry and research experience in the fields of power electronics and energy. He has served both the IEEE Power Electronics and Industrial Electronics Societies in numerous roles, relating to conferences, technical committees, and chapter activities. He is currently an Associate Editor for IEEE TRANSACTIONS ON INDUSTRIAL ELECTRONICS and IEEE TRANSACTIONS ON POWER ELECTRONICS, and a Member of the Sustainable Energy Systems Technical Committee and the Oceania Liaison Chair of Membership Development Committee of the IEEE Power Electronics Society.

Aiguo Patrick Hu (M'01–SM'07) received the B.E. and M.E. degrees from Xian JiaoTong University, Xian, China, in 1985 and 1988, respectively, and the Ph.D. degree from The University of Auckland, Auckland, New Zealand, in 2001.

Funded by Asian 2000 Foundation, he stayed in National University of Singapore as an Exchange Postdoctoral Research Fellow. He is a leading Researcher in wireless power technologies. He is a Full Professor and the Deputy Head of the Department of Electrical and Electronic Engineering, The University of Auckland. He is also the Head of Research of PowerbyProxi, Ltd., Auckland. He holds more than 50 patents in wireless power transfer and microcomputer control technologies, authored/coauthored more than 200 peer-reviewed journal and conference papers with more than 4000 citations, authored the first monograph on wireless inductive power transfer technology, and contributed four book chapters on inductive power transfer control as well as electrical machines. His research interests include wireless/contactless power transfer systems, and application of power electronics in renewable energy systems.

Dr. Hu has been a Foreign Expert Reviewer of 973 projects for the Chinese Ministry of Science and Technology, and an Assessor of ChangJiang Scholars for the Ministry of Education. He is the former Chairman of IEEE NZ Power Systems/Power Electronics Chapter. He was a recipient of the University of Auckland VC's Funded Research and Commercialization Medal in April 2017.

Chunting Chris Mi (S'00–A'01–M'01–SM'03–F'12) received the B.S.E.E. and M.S.E.E. degrees in electrical engineering from Northwestern Polytechnical University, Xi'an, China, in 1985 and 1988, and the Ph.D. degree in electrical engineering from the University of Toronto, Toronto, Ontario, Canada, in 2001.

He is a Professor of electrical and computer engineering and the Director of the Department of Energy-funded Graduate Automotive Technology Education Center for Electric Drive Transportation, San Diego State University, San Diego, CA, USA. He was a Faculty Member with the University of Michigan, Dearborn, USA, from 2001 to 2015. He was with General Electric Company, Peterborough, ON, from 2000 to 2001. He was the President and the Chief Technical Officer of Power Solutions, Inc., from 2008 to 2011. He is the Co-Founder of Mia Motors, Inc., and SNC Technology, Inc. His research interests include electric drives, power electronics, electric machines, renewable energy systems, electrical and hybrid vehicles, battery management systems, and wireless power transfer.

Dr. Mi is a recipient of the 2007 IEEE Region 4 "Outstanding Engineer Award," "IEEE Southeastern Michigan Section Outstanding Professional Award," and the "SAE Environmental Excellence in Transportation (E2T) Award." He was recipient of the IEEE TRANSACTIONS ON POWER ELECTRONICS Best Paper Award and Prize Letter Award.